

# Is disorder a friend or a foe to melting of Wigner-Mott insulators?

Mohammed Hammam,<sup>1,2,3</sup> Cyprian Lewandowski,<sup>1,2,3</sup> Vladimir Dobrosavljevic,<sup>1,2,3</sup> and Sandeep Joy<sup>1,2,3</sup>

<sup>1</sup>*National High Magnetic Field Laboratory, Tallahassee, Florida 32310, USA*

<sup>2</sup>*Department of Physics, Florida State University, Tallahassee, Florida 32306, USA*

<sup>3</sup>*FSU Quantum Initiative, Florida State University, Tallahassee, Florida 32306, USA*

(Dated: December 10, 2025)

Wigner crystals are extremely fragile, which is shown to result from very strong geometric frustration germane to long-range Coulomb interactions. Physically, this is manifested by a very small characteristic energy scale for shear density fluctuations, which are gapless excitations in a translationally invariant system. The presence of disorder, however, breaks translational invariance, thus suppressing gapless excitations and pushing them to higher density. We illustrate this general principle by explicit microscopic model calculations, showing that this mechanism very effectively stabilizes disordered Wigner lattices to much higher temperatures and densities than in the clean limit. On the other hand, we argue that in two dimensions disorder significantly “smears” the melting transition, producing spatial coexistence of solid-like and liquid-like regions – just as recently observed in STM experiments. Our results paint a new physical picture for melting of Wigner-Mott solids in two dimensions, corresponding to a Mott-Hubbard model with spatially varying local electronic bandwidth.

At very low electron densities ( $n$ ) and temperatures ( $T$ ), a spatially uniform two-dimensional electron liquid spontaneously breaks translational symmetry and forms a solid arrangement known as a Wigner crystal (WC) [1]. This phase transition arises from the competition between the interaction energy ( $E_c \sim e^2 n^{1/2} / \epsilon_r$ ), which dominates over the kinetic energy (Here  $-e < 0$  is the electron charge and  $\epsilon_r$  is the dielectric constant of the medium). The kinetic energy is either quantum mechanical ( $E_F \sim \hbar^2 n / m$ ) or thermal ( $\sim k_B T$ ), where  $\hbar$  is the reduced Planck’s constant,  $m$  is the effective mass of the electron, and  $k_B$  is the Boltzmann’s constant. Although this phenomenon was proposed nearly a century ago, direct imaging of the WC phase, along with its melting transition, has only become possible recently [2]<sup>1</sup>.

Recent experimental observations, however, reveal notable discrepancies with existing theoretical predictions. Quantum Monte Carlo (QMC) simulations predict the melting of WC’s at values of the dimensionless interaction parameter  $r_s$  (defined as  $r_s \equiv 1/(\pi n a_B^2)$ ,  $a_B = \hbar^2 \epsilon_r / m e^2$ ) around  $\sim 30$ – $34$  [5, 6]<sup>2</sup>. In contrast, experiments show that WC’s remain stable at much lower  $r_s$  values—that is, at significantly higher electron densities [8, 9]. Moreover, the experiments in Ref. [2, 10] report the existence of an intermediate phase in which both solid and liquid states coexist. Scenarios involving electronic microemulsions [11–13] and long-wavelength electron density fluctuations [14–16] have been ruled out as the origin of this observation. Instead, the enhanced stability and the intermediate phase have been attributed to short-range disorder based on the energetics argument [9].

The melting of a WC can be understood in terms of the

zero-point motion of the electrons that form the Wigner lattice: when the displacement amplitude becomes comparable to the lattice spacing, the crystal structure destabilizes and melts. This intuition lays the groundwork for the definition of the Lindemann ratio, an empirical criterion for predicting melting. In the clean limit, the Lindemann ratio has been widely used to compute phase diagrams and has proven successful in reproducing melting curves. It is defined as the ratio of the root-mean-square fluctuations around the equilibrium position to the lattice spacing. Remarkably, this ratio assumes a nearly universal value—typically between 0.20 and 0.25—across a wide range of melting transitions, whether classical or quantum, and regardless of whether the particles involved are bosons or fermions [17–19]<sup>3</sup>. This near-universal behavior of the Lindemann ratio is leveraged throughout this paper to characterize the phase diagram of the WC in the presence of disorder<sup>4</sup>.

Our main result can be summarized as follows. As expected, disorder stabilizes the WC phase to much higher densities. However, in the presence of disorder there is no sharp liquid–solid phase transition, but rather a crossover in which density fluctuations proliferate in certain regions (domains)<sup>5</sup>. This is consistent with standard Imry–Ma arguments [43]: disorder explicitly breaks translational invariance and acts as a random field coupled to the crystalline order parameter. We characterize melting through a spatially varying vibrational amplitude. Physically, when this amplitude in a given re-

<sup>1</sup> It must be noted that separate recent studies have imaged WC’s stabilized either by periodic moiré modulation [3]—often termed ‘generalized’ WC’s—or by strong magnetic fields that quench the kinetic energy [4].

<sup>2</sup> Hartree–Fock methods overestimate stability the crystalline phase and predict  $r_s$  of the order unity; see Ref. [7] for a recent analysis.

<sup>3</sup> The Lindemann ratio has been widely used in past studies of melting in the flux lattice of type-II superconductors [20–23].

<sup>4</sup> The influence of impurities on electron solids and charge-density waves has been explored extensively in earlier theoretical studies [24–36], often inspired by analogous ideas developed for pinned vortex lattices in superconductors [37–39]. However, this body of work has mainly concentrated on how impurity pinning modifies the static and dynamical properties.

<sup>5</sup> Formation of such domains has been indirectly inferred in the past from RF-conductivity experiments in magnetic field induced WC’s; see, e.g., Refs. [41, 42].

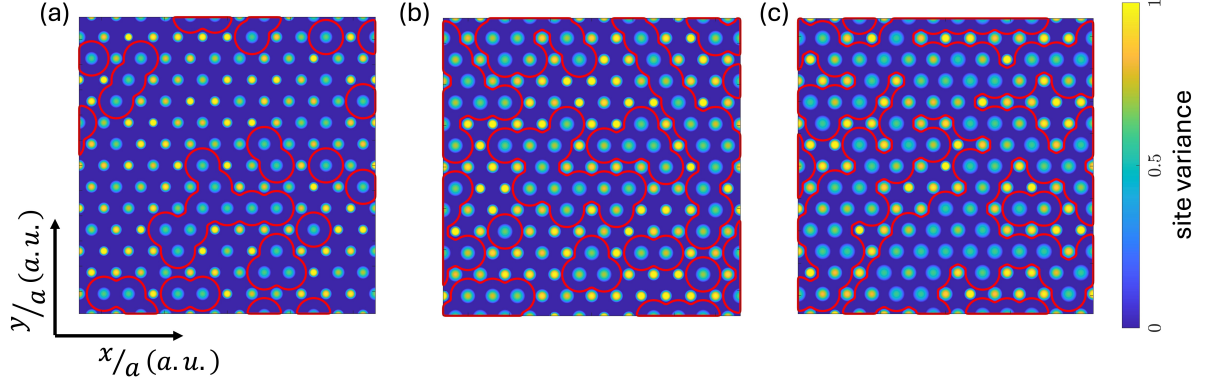


FIG. 1: This schematic figure illustrates how the fraction of melted sites increases as the electron density is tuned from low to high from left to right. The individual Gaussian wave packets are constructed using an Einstein-phonon approximation. Contour lines are drawn around regions that have locally melted; bright yellow denotes unmelted sites, whereas faded blue indicates melted sites. Here, the disorder strength used is  $x_d = 2\xi_0$ , where  $\xi_0$  is the bare bandwidth of the transverse phonon at the given density (see Ref. [40]).

gion becomes comparable to the inter-particle spacing, particles there can exchange places and move around. Owing to disorder, the associated Lindemann ratios form a probability distribution, which we compute within our formalism. This picture can be visualized by placing a Gaussian wave packet on each site, with its width set by the local fluctuation amplitude. As temperature or density increases, some Gaussians broaden earlier and begin to overlap, forming connected liquid-like regions [illustrated in Fig. 1]. These real-space patterns closely resemble STM images in experiments and provide a compelling illustration of our theoretical framework.

In order to study the melting transition, let us set up the following low-energy effective Hamiltonian of a WC in the presence of impurities:

$$H_{\text{phonon}} = \sum_i \frac{p_i^2}{2m} + \frac{1}{2} \sum_{i,j,\alpha,\beta} u_i^\alpha D_{ij}^{\alpha\beta} u_j^\beta + \frac{1}{2} \sum_i \kappa_i u_i^2. \quad (1)$$

Here,  $u_i$  denotes the displacement of the electron at site  $i$  from its equilibrium position, and  $D_{ij}^{\alpha\beta}$  is the dynamical matrix coupling fluctuations at sites  $i$  and  $j$  along directions  $\alpha$  and  $\beta$ . The explicit form of  $D_{ij}^{\alpha\beta}$  for a triangular WC is given in the supplemental material [40]. The last term accounts for disorder, with  $\kappa_i$  representing the local onsite pinning potential. The physical intuition behind this disorder term is that, in the presence of atomic-scale, short-ranged defects—such as those relevant in STM experiments—the disorder length scale is much smaller than the spatial extent of the WC electron wave packet. Impurities that lie within a given wave packet effectively pin the electron locally, enhancing its con-

finement relative to the clean limit<sup>6</sup>. We assume a Gaussian distribution for  $\kappa_i$ . As shown in the supplemental material, our results are qualitatively insensitive to the specific choice of disorder distribution, and we also derive the effective form of the disorder potential from first principles in the limit of weak, short-ranged disorder [40].

Here we first briefly discuss the physics of WC melting in the absence of disorder, before turning to the disorder-dominated case (in the process, we will introduce the Lindemann ratio). The theory of two-dimensional crystals has a long history (see Ref. [44] for a review). Melting of a 2D WC, however, is more subtle than that of ordinary 2D solids, owing to the fermionic nature of electrons, their spin degrees of freedom, and the long-range Coulomb interaction. Nevertheless, the Lindemann ratio serves as a remarkably effective tool for understanding the melting of a WC [17–19]. Its effectiveness is not accidental—although we do not attempt a first-principles derivation here. The key idea is that melting is governed by the collective Goldstone modes of the crystal. The dominant thermal or quantum fluctuations are the harmonic vibrational modes of the WC, with the shear mode setting the relevant Debye energy scale [45, 46]. It is important to note that, since the crystal is two-dimensional, it supports two phonon modes: a transverse phonon with a linear dispersion,  $\omega_{T,q} \sim q$ , and a longitudinal phonon with

<sup>6</sup> Experiments in Refs. [2, 10] also indicate the presence of long-ranged disorder arising from Coulomb impurities. Even in the presence of Coulomb disorder, an effective phonon model should still be possible. This might imply some degree of correlation between disorder on different sites, given the longer range of the Coulomb interaction, we leave an exploration of these effects to future work [29].

$\omega_{L,q} \sim \sqrt{q}$ <sup>7</sup>. Since the shear mode is far softer than the longitudinal mode for WC's, the melting is predominantly governed by transverse fluctuations. We have compared the melting boundary obtained by including both phonon modes with that obtained by considering only the transverse fluctuations and found that the two agree with high accuracy, as shown in the supplemental material [40]. In the rest of the paper, we will restrict ourselves to discussing transverse phonons when examining the melting.

As discussed in the introduction, conventionally the Lindemann ratio is defined as  $\eta_{\text{site}}^2 \equiv \sigma_{\text{site}}^2/a^2$ , where

$$\sigma_{\text{site}}^2 = \frac{1}{N} \sum_i \langle \mathbf{u}_i^2 \rangle. \quad (2)$$

Here,  $i$  is the index of the site in the Wigner lattice in real space, and  $N$  is the total number of sites. The subscript “site” refers to the fact that this involves fluctuations of the sites, and it becomes clearer why we used that below. One can rewrite this in the momentum space in terms of the normal phonon modes as follows:

$$\sigma_{\text{site}}^2 = a_c \int \frac{d^2 \mathbf{q}}{(2\pi)^2} \left( \frac{\hbar}{2m\omega_q} \right) \coth \left[ \frac{\hbar\omega_q}{2k_B T} \right], \quad (3)$$

where  $a_c = \sqrt{3}a^2/2$  is the area of the unit cell of the Wigner lattice.  $\sigma_{\text{site}}^2$  is a well defined quantity at  $T = 0$ <sup>8</sup>. However, at finite  $T$ , this momentum integral diverges logarithmically with the infrared cut-off at finite temperature  $\sim T \log(1/q_{\min}a)$ , where  $q_{\min}$  is the lower cut-off of the integral, as dictated by the Mermin–Wagner theorem [19]. This divergence prohibits us from using this to find the finite temperature melting point. One can alternatively define a generalized Lindemann ratio that measures relative (bond) fluctuations [47–49].

$$\sigma_{\text{bond}}^2 \equiv \frac{1}{2NM} \sum_{i,j \in NN} \sum_a \langle (u_i^a - u_j^a)^2 \rangle \quad (4)$$

Here  $M = 6$  is the number of nearest neighbors. Equation (4) can be written in terms of the (shear) phonon modes as follows:

$$\sigma_{\text{bond}}^2 = \frac{a_c}{2M} \int \frac{d^2 \mathbf{q}}{(2\pi)^2} \left( \frac{\hbar}{2m\omega_{\alpha,q}} \right) \coth \left[ \frac{\hbar\omega_{\alpha,q}}{2k_B T} \right] f(\mathbf{q}) \quad (5)$$

Here  $f(\mathbf{q})$  is the following geometrical factor:

$$f(\mathbf{q}) = \sum_{j \in NN} 4 \sin^2 \left( \frac{\mathbf{q} \cdot \mathbf{b}_j}{2} \right). \quad (6)$$

The vectors  $\mathbf{b}_j$  point towards the nearest neighbor lattice sites. This approach effectively removes the logarithmic divergence by introducing a soft cut-off<sup>9</sup> (in the limit  $q \rightarrow 0$ ,  $f(\mathbf{q})$  can be expanded as,  $\approx 3q^2/4$ ). Following the literature where  $\eta_{\text{site}}^c \approx 0.23$  [18], corresponding  $\eta_{\text{bond}}^c \approx 0.25$  so that they reproduce the same zero temperature melting line. We note that this indicates the physics of 2D WC melting is controlled by the UV energy scale—specifically, the Debye energy or, equivalently, the large- $q$  contributions. This scale is the same in all dimensions, highlighting the distinctive nature of WC melting. This observation motivates our use of the Einstein-phonon approximation later for generating real-space charge-density plots.

When dealing with disorder, it is more convenient to work in the language of Green's functions. In the remainder of the paper, we therefore use the following retarded Green's function:<sup>10</sup>

$$G_{j_1 j_2}(t) \equiv -i\theta(t) \langle [u_{j_1}(t), u_{j_2}(0)] \rangle \quad (7)$$

Here  $\langle \cdot \rangle$  denotes the finite temperature expectation value. In terms of the Green's function, relative bond fluctuations can be written as follows:

$$\sigma_{\text{bond}}^2 = \frac{a_c}{2M} \sum_a \int \frac{d\mathbf{q}}{(2\pi)^2} \int_{-\infty}^{\infty} \frac{d\omega}{2\pi} n_B(\omega) B(\mathbf{q}, \omega) f(\mathbf{q}) \quad (8)$$

where

$$B(\mathbf{q}, \omega) \equiv -2\text{Im}(G(\mathbf{q}, \omega)), \quad (9)$$

is the (bosonic) spectral function. We will also define a local Lindemann ratio as:

$$\sigma_{\text{bond-local}}^2 = \frac{1}{2M} \sum_{i \in NN} \langle (u_0 - u_i)^2 \rangle \quad (10)$$

In the clean limit, this quantity is equivalent to the spatially averaged quantity. However, in the case of a disordered situation, this quantity exhibits spatial fluctuations. We will be using Eq. (10) as a measure later to estimate the fraction of melted sites to construct the phase diagram. In terms of the Green's function language, this quantity is given by:

$$\sigma_{\text{bond-local}}^2 = \frac{1}{2} \int_{-\infty}^{\infty} \frac{d\omega}{2\pi} n_B(\omega) (B_{\kappa_0}(\omega) - \bar{B}(\omega)) + \sigma_{\text{bond}}^2 \quad (11)$$

Here  $B_{\kappa_0}(\omega)$  is the local spectral function as a function of the local pinning  $\kappa_0$ , and  $\bar{B}(\omega)$  is the disorder-averaged local spectral function.

We calculate the Green's function needed for the Lindemann ratio using dynamical mean-field theory within the coherent potential approximation (DMFT-CPA) [53–58]. This

<sup>7</sup> This is the plasmon mode that arises from the long-range nature of the Coulomb interactions and also exists in the liquid phase.

<sup>8</sup> At  $T = 0$ , this is a 2 + 1D quantum theory, which maps to a 3D classical theory that is not subject to the curse of Mermin–Wagner theorem. In Eq. (3), this corresponds to  $\coth(\infty) = 1$ , ensuring that the integral has no infrared divergence.

<sup>9</sup> In this sense, previous harmonic oscillator (HO) approaches [50–52] can be interpreted as focusing on relative fluctuations: it effectively pins all other electrons in place when computing the confining potential.

<sup>10</sup> We are only considering the transverse fluctuations here.

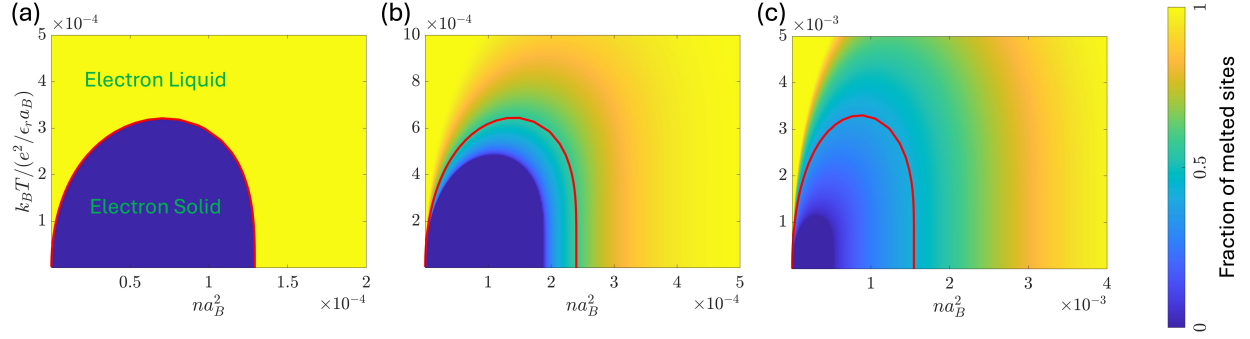


FIG. 2: The phase diagram of a two-dimensional electron system as a function of electron density and temperature for different disorder strengths. The solid red line denotes the melting line estimated from the global (bond) Lindemann ratio. The color gradient indicates the fraction of melted sites, calculated from the local (bond) Lindemann ratio. The color gradient goes from blue (dark shade) at zero to yellow (light shade) at one. The disorder strength is given in units of  $\xi_0$ , which is the bare bandwidth of the transverse phonon at the given density. (a) The clean limit is presented where there is “nominally” a phase transition expected. (b) The disorder strength is given by  $x_d = 0.5 \xi_0$  (c) The disorder strength is given by  $x_d = 2 \xi_0$ . As discussed in the main text, in the presence of disorder—which breaks translational symmetry—the melting/freezing transition that usually distinguishes a solid from a liquid is no longer well defined. Therefore, we do not label the phases in that way in the figures. (b) and (c).

approach has been most commonly applied to study strong correlations and disorder in fermionic systems; however, its application to bosonic systems also exists (see, e.g., Refs. [59–61]). For a bosonic system, the Green’s function can be written as:

$$G(z) = \int_0^{\xi_0} d\xi \frac{\rho_0(\xi)}{z^2 - \Sigma(z) - \xi^2}. \quad (12)$$

Here  $z = \omega + i0^+$  denotes the complex frequency, with  $\omega$  as the real frequency and  $0^+$  an infinitesimally small positive number ensuring causality. The integration variable  $\xi$  denotes energy, and  $\rho_0(\xi)$  is the bare density of states (The details specific to the triangular WC are given in the supplemental material [40]). The quantity  $\Sigma(z)$  is the self-consistent self-energy, which can be calculated locally within DMFT-CPA, and encodes the modification of the bare spectrum induced by disorder<sup>11</sup>. The next step in DMFT-CPA involves introducing a self-consistent cavity field  $\Delta(z)$  which relates the Green’s function to the distribution of the disorder as follows:

$$G(z) = \int dx \frac{P(x)}{z^2 - \Delta(z) - x^2} \quad (13)$$

Here  $x$  is related to the onsite pinning as  $x = \sqrt{\kappa_i/m}$ . One has to solve for the cavity field using the following relation:

$$\Delta(z) = z^2 - \Sigma(z) - G^{-1}(z) \quad (14)$$

Details about the numerical techniques are provided in the supplemental material [40].

Now that we have introduced the essential tools, we present our results. In Fig. 2, we show the phase diagram of the WC in the density–temperature plane. Figure 2(a) corresponds to the clean limit, where the Lindemann ratio indicates a sharp melting transition<sup>12</sup>. The colors—blue (dark) to yellow (light)—represent the fraction of melted sites ranging from zero to one. As the strength of disorder increases, two apparent effects emerge. First, the solid line—representing the spatially averaged Lindemann ratio—shows that the crystal becomes stabilized to much higher densities, as seen in Fig. 2(b) and Fig. 2(c), corresponding to weak and strong disorder, respectively. Second, around this line, a broad region exists where the fraction of melted sites varies continuously from zero to one, indicating that there is no longer a sharp melting transition.

In Fig. 3(a) we demonstrate that the average local bond fluctuation decreases as the disorder strength increases. This quantity saturates at large  $x$  due to the presence of the constant term in Eq. (11). Figure 3(b) shows the probability distribution of the local bond Lindemann ratios. Each curve exhibits a (removable) singularity at the maximum allowed value of the local Lindemann ratio, which occurs at  $x = 0$ .

<sup>11</sup>  $\Sigma(z)$  vanishes in the clean limit. In that case, Eq. (12) simply reproduces the real-frequency Green’s function obtained by Fourier transforming the momentum-space propagator.

<sup>12</sup> Even in the clean limit, a direct first-order transition is replaced (possibly) by a series of intermediate electronic microemulsion phases owing to the long-range nature of the interactions. However, the window of such intermediate phases are extremely narrow [62].



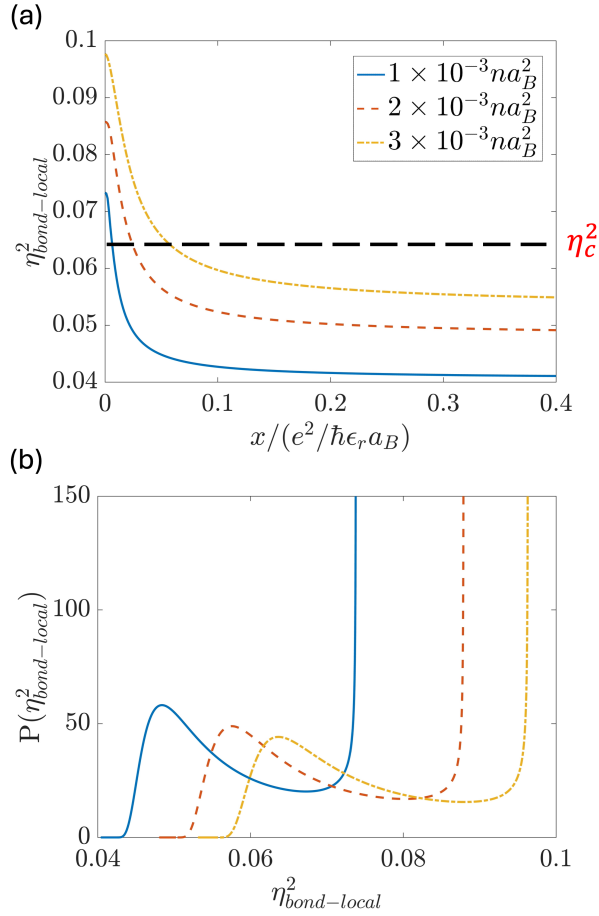


FIG. 3: (a) The local (bond) Lindemann ratio is plotted against the local disorder strength for three different densities at  $x_d = 2\xi_0$ . The horizontal black dashed line marks the critical Lindemann ratio at which local melting occurs, implying that, depending on the local disorder strength, different lattice sites can undergo melting independently. (b) The probability distributions of the local bond Lindemann ratio for these same disorder strengths are numerically calculated and shown here.

This behavior reflects the fact that  $P(x)$  and  $\eta_{\text{bond-local}}^2$  peaks at  $x = 0$ <sup>13</sup>.

The absence of a sharp transition is further illustrated in Fig. 1, where we present real-space images. We construct a triangular lattice (used as an approximation to the triangulation observed experimentally) and sample local site fluctuations using the same Gaussian disorder as before. We have utilized the Einstein-phonon approximation to create this wave packet since  $\langle u_i^2 \rangle$  nominally diverges at finite temperatures in the clean limit. The details of this construction

are provided in the supplemental material [40]. As the density increases (left to right), the number of sites satisfying the local Lindemann melting criterion grows, forming a percolating cluster or melted region—similar to what is seen in experiments. However, we emphasize that our theory, which relies on the Lindemann criterion, cannot reliably describe the melted regime. We can only assert that the system is no longer a solid; the nature of the melted phase (presumably a liquid with strong short-range correlations) is beyond the scope of our current description.

We conclude by saying that a frozen spatial charge profile—whether from STM or simulations—cannot sharply identify a “melting” transition in terms of density (equivalently  $r_s$ ) or temperatures. There are past experiments on the WC melting transition—using transport and optical spectroscopy—that report intermediate phases not consistent with either a conventional WC or a Fermi liquid (see e.g., Refs. [63–69]). These observations can be explained by the disorder-induced coexistence of clustered solid and liquid domains that we have found. However, there could be a well-defined transition: an insulator-metal transition (IMT), widely observed in two-dimensional electron systems as density is varied (pinned WC is an insulator, thus undergoes an IMT upon melting). We speculate that this IMT is Mott-like in nature. In the insulating phase, each WC site hosts a single localized electron forming a local moment, whereas the metallic phase is a disordered Fermi liquid [70–72].

We note that after this work was completed, a related joint experiment–theory preprint [10] appeared, using STM and QMC to investigate disorder effects on the WC. Their findings are consistent with our predictions.

**Acknowledgments.** The authors are grateful to Ilya Esterlis, Zhehao Ge, Steve Kivelson, and Brian Skinner for useful discussions. S.J. acknowledges support from Florida State University through the Quantum Postdoctoral Fellowship and the National High Magnetic Field Laboratory. C.L. was supported by start-up funds from Florida State University and the National High Magnetic Field Laboratory. M. H. and V. D. were supported by the NSF Grant No. DMR-2409911 and the National High Magnetic Field Laboratory. The National High Magnetic Field Laboratory is supported by the National Science Foundation through NSF/DMR-2128556 and the State of Florida.

- 
- [1] E. Wigner, *Phys. Rev.* **46**, 1002 (1934).
  - [2] Z. Xiang, H. Li, J. Xiao, M. H. Naik, Z. Ge, Z. He, S. Chen, J. Nie, S. Li, Y. Jiang, R. Sailus, R. Banerjee, T. Taniguchi, K. Watanabe, S. Tongay, S. G. Louie, M. F. Crommie, and F. Wang, *Science* **388**, 736 (2025).
  - [3] H. Li, S. Li, E. C. Regan, D. Wang, W. Zhao, S. Kahn, K. Yumigeta, M. Blei, T. Taniguchi, K. Watanabe, S. Tongay, A. Zettl, M. F. Crommie, and F. Wang, *Nature* **597**, 650 (2021).
  - [4] Y.-C. Tsui, M. He, Y. Hu, E. Lake, T. Wang, K. Watanabe,

<sup>13</sup> It is noteworthy that a local maximum emerges at finite  $\eta_{\text{bond-local}}^2$ . We attribute this to the convolution involved in mapping  $P(x)$  to  $P(\eta_{\text{bond-local}}^2)$ .

- T. Taniguchi, M. P. Zaletel, and A. Yazdani, *Nature* **628**, 287 (2024).
- [5] N. D. Drummond and R. J. Needs, *Phys. Rev. Lett.* **102**, 126402 (2009).
- [6] B. K. Clark, M. Casula, and D. M. Ceperley, *Phys. Rev. Lett.* **103**, 055701 (2009).
- [7] A. Jain and C. Huang, “Elementary excitations, melting temperature and correlation energy in wigner crystal,” (2025), [arXiv:2504.04538](#).
- [8] Y. Huang and S. Das Sarma, *Phys. Rev. B* **109**, 245431 (2024).
- [9] S. Joy and B. Skinner, “Disorder-induced liquid-solid phase coexistence in 2D electron systems,” (2025), [arXiv:2502.11235](#).
- [10] Z. Ge, C. Smith, Z. He, Y. Yang, Q. Li, Z. Xiang, J. Xiao, W. Zhou, S. Kahn, M. Erdi, R. Banerjee, T. Taniguchi, K. Watanabe, S. A. Tongay, M. A. Morales, S. Zhang, F. Wang, and M. F. Crommie, “Visualizing the impact of quenched disorder on 2d electron wigner solids,” (2025), [arXiv:2510.12009](#).
- [11] B. Spivak, *Phys. Rev. B* **67**, 125205 (2003).
- [12] B. Spivak and S. A. Kivelson, *Phys. Rev. B* **70**, 155114 (2004).
- [13] R. Jamei, S. Kivelson, and B. Spivak, *Phys. Rev. Lett.* **94**, 056805 (2005).
- [14] B. I. Shklovskii and A. L. Efros, *Sov. Phys.-JETP* **35**, 610 (1972).
- [15] T. Ando, A. B. Fowler, and F. Stern, *Rev. Mod. Phys.* **54**, 437 (1982).
- [16] B. I. Shklovskii, *Phys. Rev. B* **76**, 233411 (2007).
- [17] G. E. Astrakharchik, J. Boronat, I. L. Kurbakov, and Y. E. Lozovik, *Phys. Rev. Lett.* **98**, 060405 (2007).
- [18] M. Babadi, B. Skinner, M. M. Fogler, and E. Demler, *EPL (Europhysics Letters)* **103**, 16002 (2013).
- [19] S. A. Khrapak, *Phys. Rev. Res.* **2**, 012040 (2020).
- [20] E. H. Brandt, *Phys. Rev. Lett.* **63**, 1106 (1989).
- [21] A. Houghton, R. A. Pelcovits, and A. Sudbø, *Phys. Rev. B* **40**, 6763 (1989).
- [22] D. R. Nelson and H. S. Seung, *Phys. Rev. B* **39**, 9153 (1989).
- [23] D. S. Fisher, M. P. A. Fisher, and D. A. Huse, *Phys. Rev. B* **43**, 130 (1991).
- [24] H. Fukuyama and P. A. Lee, *Phys. Rev. B* **17**, 535 (1978).
- [25] P. A. Lee and H. Fukuyama, *Phys. Rev. B* **17**, 542 (1978).
- [26] H. Fukuyama and P. A. Lee, *Phys. Rev. B* **18**, 6245 (1978).
- [27] P. A. Lee and T. M. Rice, *Phys. Rev. B* **19**, 3970 (1979).
- [28] B. G. A. Normand, P. B. Littlewood, and A. J. Millis, *Phys. Rev. B* **46**, 3920 (1992).
- [29] I. M. Ruzin, S. Marianer, and B. I. Shklovskii, *Phys. Rev. B* **46**, 3999 (1992).
- [30] M.-C. Cha and H. A. Fertig, *Phys. Rev. Lett.* **73**, 870 (1994).
- [31] M.-C. Cha and H. A. Fertig, *Phys. Rev. B* **50**, 14368 (1994).
- [32] R. Chitra, T. Giamarchi, and P. Le Doussal, *Phys. Rev. Lett.* **80**, 3827 (1998).
- [33] H. A. Fertig, *Phys. Rev. B* **59**, 2120 (1999).
- [34] M. M. Fogler and D. A. Huse, *Phys. Rev. B* **62**, 7553 (2000).
- [35] R. Chitra, T. Giamarchi, and P. Le Doussal, *Phys. Rev. B* **65**, 035312 (2001).
- [36] R. Chitra and T. Giamarchi, *Eur. Phys. J. B* **44**, 455 (2005).
- [37] A. I. Larkin, *Sov. Phys.-JETP* **31**, 784 (1970).
- [38] A. Larkin and Y. N. Ovchinnikov, *Journal of Low Temperature Physics* **34**, 409 (1979).
- [39] G. Blatter, M. V. Feigel'man, V. B. Geshkenbein, A. I. Larkin, and V. M. Vinokur, *Rev. Mod. Phys.* **66**, 1125 (1994).
- [40] Supplemental materials will be uploaded soon.
- [41] B.-H. Moon, L. W. Engel, D. C. Tsui, L. N. Pfeiffer, and K. W. West, *Phys. Rev. B* **89**, 075310 (2014).
- [42] M. L. Freeman, P. T. Madathil, L. N. Pfeiffer, K. W. Baldwin, Y. J. Chung, R. Winkler, M. Shayegan, and L. W. Engel, *Phys. Rev. Lett.* **132**, 176301 (2024).
- [43] Y. Imry and S. K. Ma, *Phys. Rev. Lett.* **35**, 1399 (1975).
- [44] K. J. Strandburg, *Rev. Mod. Phys.* **60**, 161 (1988).
- [45] D. J. Thouless, *J. Phys. C: Solid State Phys.* **11**, L189 (1978).
- [46] D. S. Fisher, *Phys. Rev. B* **26**, 5009 (1982).
- [47] Y. Lozovik and V. Farztdinov, *Solid State Commun.* **54**, 725 (1985).
- [48] V. Bedanov, G. Gadiyak, and Y. Lozovik, *Phys. Lett. A* **109**, 289 (1985).
- [49] G. Goldoni and F. M. Peeters, *Phys. Rev. B* **53**, 4591 (1996).
- [50] S. Joy and B. Skinner, *Phys. Rev. B* **106**, L041402 (2022).
- [51] S. Joy and B. Skinner, “Wigner crystallization in bernal bilayer graphene,” (2023), [arXiv:2310.07751](#).
- [52] S. Joy, L. Levitov, and B. Skinner, [arXiv:2507.22121](#).
- [53] J. Korrington, *J. Phys. Chem. Solids* **7**, 252 (1958).
- [54] J. L. Beeby, *Phys. Rev.* **135**, A130 (1964).
- [55] P. Soven, *Phys. Rev.* **156**, 809 (1967).
- [56] A. Georges, G. Kotliar, W. Krauth, and M. J. Rozenberg, *Rev. Mod. Phys.* **68**, 13 (1996).
- [57] S. Pankov, G. Kotliar, and Y. Motome, *Phys. Rev. B* **66**, 045117 (2002).
- [58] S. Ciuchi, D. Di Sante, V. Dobrosavljević, and S. Fratini, *npj Quantum Materials* **3**, 44 (2018).
- [59] S. Ghosh, P. L. Leath, and M. H. Cohen, *Phys. Rev. B* **66**, 214206 (2002).
- [60] W. R. Mondal, N. S. Vidhyadhiraja, T. Berlijn, J. Moreno, and M. Jarrell, *Phys. Rev. B* **96**, 014203 (2017).
- [61] W. R. Mondal, T. Berlijn, M. Jarrell, and N. S. Vidhyadhiraja, *Phys. Rev. B* **99**, 134203 (2019).
- [62] S. Joy and B. Skinner, *Phys. Rev. B* **108**, L241110 (2023).
- [63] J. Yoon, C. C. Li, D. Shahar, D. C. Tsui, and M. Shayegan, *Phys. Rev. Lett.* **82**, 1744 (1999).
- [64] T. Knighton, Z. Wu, J. Huang, A. Serafin, J. S. Xia, L. N. Pfeiffer, and K. W. West, *Phys. Rev. B* **97**, 085135 (2018).
- [65] S. Li, Q. Zhang, P. Ghaemi, and M. P. Sarachik, *Phys. Rev. B* **99**, 155302 (2019).
- [66] M. S. Hossain, M. K. Ma, K. A. V. Rosales, Y. J. Chung, L. N. Pfeiffer, K. W. West, K. W. Baldwin, and M. Shayegan, *PNAS* **117**, 32244 (2020).
- [67] J. Falson, I. Sodemann, B. Skinner, D. Tabrea, Y. Kozuka, A. Tsukazaki, M. Kawasaki, K. von Klitzing, and J. H. Smet, *Nature Materials* **21**, 311 (2022).
- [68] F. Yang, R. Bai, A. A. Zibrov, S. Joy, T. Taniguchi, K. Watanabe, B. Skinner, M. O. Goerbig, and A. F. Young, *Phys. Rev. Lett.* **131**, 226501 (2023).
- [69] J. Sung, J. Wang, I. Esterlis, P. A. Volkov, G. Scuri, Y. Zhou, E. Brutschea, T. Taniguchi, K. Watanabe, Y. Yang, M. A. Morales, S. Zhang, A. J. Millis, M. D. Lukin, P. Kim, E. Demler, and H. Park, *Nature Physics* (2025).
- [70] A. Camjayi, K. Haule, V. Dobrosavljević, and G. Kotliar, *Nature Physics* **4**, 932 (2008).
- [71] S. Kravchenko, *Strongly Correlated Electrons in Two Dimensions* (Jenny Stanford Publishing, 2017).
- [72] Y. Tan, V. Dobrosavljević, and L. Rademaker, *Crystals* **12** (2022), [10.3390/cryst12070932](#).